

Transfer Learning for Brain Tumor Segmentation

Jonas Wacker, Marcelo Ladeira, and José Eduardo Vaz Nascimento.

Abstract—Gliomas are the most common malignant brain tumors that are treated with chemoradiotherapy and surgery. Magnetic Resonance Imaging (MRI) is used by radiotherapists to manually segment brain lesions and to observe their development throughout the therapy. The manual image segmentation process is time-consuming and results tend to vary among different human raters. Therefore, there is a substantial demand for automatic image segmentation algorithms that produce a reliable and accurate segmentation of various brain tissue types. Recent advances in deep learning have led to convolutional neural network architectures that excel at various visual recognition tasks. They have been successfully applied to the medical context including medical image segmentation. In particular, fully convolutional networks (FCNs) such as the U-Net produce state-of-the-art results in the automatic segmentation of brain tumors. MRI brain scans are volumetric and exist in various co-registered modalities that serve as input channels for these FCN architectures. Training algorithms for brain tumor segmentation on this complex input requires large amounts of computational resources and is prone to overfitting. In this work, we construct FCNs with pretrained convolutional encoders. We show that we can stabilize the training process this way and produce more robust predictions. We evaluate our methods on publicly available data as well as on a privately acquired clinical dataset. We also show that the impact of pretraining is even higher for predictions on the clinical data.

Index Terms—Magnetic resonance imaging, Image segmentation, Convolutional neural networks, Transfer Learning.

I. INTRODUCTION

According to the American Brain Tumor Association¹, in the United States alone, each year 68,470 people are diagnosed with a primary brain tumor and more than twice that number is diagnosed with a metastatic tumor. Gliomas belong to the group of primary brain tumors and represent around 28% of all brain tumors. About 80% of all the malignant (cancerous) tumors are gliomas, which makes them the most common malignant kind. They can be divided into low-grade (WHO grade II) and high-grade (WHO grades III-IV) gliomas [1], conforming to the World Health Organization (WHO) classification.

Patients with the more aggressive high-grade gliomas (anaplastic astrocytomas and glioblastoma multiforme) have a median survival-rate of two years or less – even with aggressive chemoradiotherapy and surgery. The more slowly-

growing low-grade (astrocytomas or oligodendrogliomas) variant comes with a life expectancy of several years [2].

In any case, Magnetic Resonance Imaging (MRI) modalities are used by radiotherapists before and during the treatment process. Brain tumor regions can be manually segmented into heterogeneous sub-regions (i.e., edema, enhancing and non-enhancing core) that become visible when comparing MRI modalities with different contrast levels [3]. Commonly employed MRI modalities include T1 (spin-lattice relaxation), T1c (contrast-enhanced), T2 (spin-spin relaxation), Fluid-Attenuated Inversion Recovery (FLAIR) and many others. Each modality corresponds to gray-scale images that highlight different kinds of tissue.

The Brain Tumor Segmentation (BraTS) benchmark [2] revealed that there is a high disagreement among medical specialists when delineating the boundaries of various tumor subregions. Furthermore, the appearance of gliomas varies strongly among patients regarding shape, location and size.

Therefore, the segmentation task is considered quite challenging, especially when intensity gradients between lesions and healthy tissue are smooth. This is often the case since gliomas are infiltrative tumors.

Due to the high level of difficulty and the time-consuming nature of the task, there has been an emerging need for automatic segmentation methods over the last years. The goal of the BraTS benchmark is to compare these methods on a publicly available dataset. The data contains pre-operative multimodal MRI scans of high-grade (glioblastoma) and low-grade glioma patients acquired from 19 different institutions.

Fig. 1 shows the four MRI modalities used in BraTS of an example patient along with the ground-truth annotations.

State-of-the-art methods for automatic brain tumor segmentation use fully-convolutional networks (FCNs) such as the U-Net [4] and its volumetric extensions (e.g. V-Net [5]). A major challenge in this regard is the volumetric multi-modal input that leads to high memory requirements and long training times despite the use of expensive GPUs. For example, the third-place solution [6] for BraTS '17 took one day of training on a recent GPU for each of the five networks that were used.

In this work, we apply FCNs with encoders that are pre-trained on the well-known ImageNet large-scale image dataset [7] in order to stabilize the training process and to improve prediction performance. This approach has led to outstanding results in two-dimensional image segmentation benchmarks such as the Carvana Image Masking Challenge². The resulting U-Net architecture is called TernaNet [8]. We show that despite the difference between the ImageNet dataset and the MRI images used in this work, a considerable performance gain can be achieved while stabilizing training convergence.

This work was supported in part by the Coordenação de Aperfeiçoamento de Pessoal de Nível Superior – Brasil (CAPES) – Finance Code 001.

J. Wacker was with the University of Brasília-DF, Brazil. He is now with EURECOM University in France (corresponding author email: jonas.wacker@gmail.com).

M. Ladeira is with University of Brasília, Brasília-DF, Brazil. (email: mladeira@unb.br).

J. E. V. Nascimento is with University of Brasília, Brasília-DF, Brazil, and the Syrian-Lebanese Hospital in Brasília. (email: eduvant@yahoo.com.br).

¹<https://www.abta.org>

²<https://www.kaggle.com/c/carvana-image-masking-challenge>

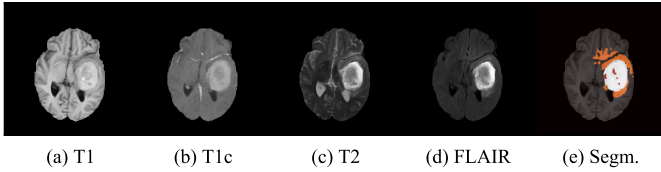


Fig. 1. Example of high-grade glioma case. The four MRI modalities (T1, T1c, T2, and FLAIR) of a single patient are shown (a-d). The rightmost image (e) shows the tumor segmentation. Orange corresponds to edema, white to the tumor core and red to the active tumor region.

Furthermore, we compare the performance of our model to the BraTS’17 winning method. The PyTorch implementation of our method is publicly available on GitHub³.

In order to further evaluate our approach in a practical context, we have acquired MRI scans of five glioma patients from the Syrian-Lebanese hospital in Brasilia (Brazil) that we consider compatible with the BraTS data. We aligned this data with the scans of the BraTS challenge, which allows us to test our method on data that comes from an institution that did not provide any training or validation data. Apart from demonstrating the predictive performance of the models in a real-world clinical setting, we also give a detailed explanation of how to convert the clinical data into a BraTS-compatible format.

In Section II, we present related brain tumor segmentation approaches that give valuable insights about the challenges that come with this task. We introduce our own approach in Section III as well as our privately acquired clinical dataset in Section IV. The evaluation of our method is carried out in Section V. Final conclusions are drawn in Section VI.

II. RELATED WORK

A. Automatic Brain Tumor Segmentation

According to Menze *et al.* [2], automatic brain tumor segmentation approaches can be divided into generative probabilistic models and discriminative methods. Generative methods incorporate prior knowledge about the structure of various tissue types and their spatial distribution. This way, tumor segmentation can be treated as anomaly detection when assuming an appropriate probabilistic model for the expected tissue appearance.

In more recent approaches of brain tumor segmentation, discriminative methods are preferred over generative ones [2]. This is due to the fact that generative models require a high degree of domain-specific knowledge, which makes the models inflexible when being applied to other types of tissue segmentation tasks. For gliomas in particular, it is quite difficult to model a prior distribution because of their strong variations in appearance.

In contrast, discriminative models do not incorporate a strong prior assumption on the data distribution but learn to distinguish between healthy tissue and lesions after having observed a large number of annotated training examples.

In earlier brain tumor segmentation competitions (e.g. BraTS ’12-’14), the most successful discriminative methods

were based on random forest classifiers applied to hand-crafted visual features (c.f. [9][10][11]).

A drawback of hand-designed features is that they need to be carefully selected and compared while mostly capturing only general patterns in images. Convolutional Neural Networks (CNNs) have proven to be able to *learn* domain-specific image features automatically and produce state-of-the-art results in image classification tasks such as the ImageNet classification challenge [7].

CNNs have been successfully applied to image segmentation tasks where a “fully convolutional network” (FCN) outperformed previous approaches by a large margin [12]. An FCN is a CNN that uses *only* convolutional layers. Moreover, the FCN is characterized by fast prediction times segmenting a whole image at once instead of classifying one pixel at a time, which comes at the cost of high memory requirements. This line of research paved the way for the U-Net architecture [4] that is specifically designed for image segmentation in a medical context. The U-Net achieved best results in two medical image segmentation challenges [13][14] while having shorter prediction times than the original FCN presented in [12]. However, the traditional U-Net is limited to two-dimensional inputs. U-Net inspired architectures for volumetric inputs have therefore been proposed (e.g. [5][6][15][16]).

B. Transfer Learning for Image Segmentation

Transfer Learning has become a very popular technique in image classification tasks. In particular, off-the-shelf convolutional features have shown to be a better classifier input than traditional hand-crafted image descriptors for many datasets [17]. These features are learned automatically by training convolutional neural networks on large-scale image datasets such as ImageNet [7]. Especially in situations where only little training data is available, results can be improved by extracting convolutional features for the data at hand and training a classifier on them or by fine-tuning existing CNNs.

Being widely used in image classification, transfer learning has only recently been introduced to image segmentation tasks with the so-called TerausNet architecture [8].

It turns out that pretrained convolutional layers of classification CNNs can be treated as a downsampling path (encoder) in U-Net architectures for image segmentation. Only the upsampling path (decoder) is trained from scratch, which leads to improved segmentation results and sometimes faster convergence. The TerausNet approach has won various image segmentation competitions including the Carvana Image Masking Challenge⁴ and the MICCAI 2017 Endoscopic Vision Challenge [18].

There is little prior work on applying transfer learning to MRI data. Previous work includes transfer learning for MRI image classification [19] and Brain Lesion Segmentation with a network that was pre-trained in the same domain [20]. The closest method to ours extends a DenseNet encoder that was pretrained on the ImageNet dataset in order to segment the BraTS data [21]. The major difference is that the authors treat a stack of three input slices corresponding to a single

³<https://github.com/joneswack/brats-pretraining>

⁴<https://www.kaggle.com/c/carvana-image-masking-challenge>

MRI modality as RGB channels. Therefore, a forward pass through DenseNet takes place for each of the four modalities. The resulting features are then combined in the decoder. Instead, our approach provides end-to-end learning with a single forward pass and can be extended to process volumes of arbitrary depth. Moreover, we carry out a detailed analysis about the impact of the pretraining on a public as well as on a clinical dataset which has not been done before.

III. METHODOLOGY

A. Extending the AlbuNet architecture

We make use of a ResNet34 [22] encoder that results in the AlbuNet variant [23] of TerausNet. Fig. 2 depicts our U-Net based architecture. The ResNet34 downsampling layers are complemented with an upsampling path that uses transpose convolutional layers and receives intermediate inputs from the downsampling path. Both paths are symmetric in the dimensionality of intermediate outputs that they produce. However, no residual connections are used in the upsampling path that also contains less convolutional layers than the downsampling path.

In order to match the expected RGB three-channel input of the ResNet34 architecture, we select only the T1c, T2 and FLAIR modalities and discard T1 scans. We then normalize voxel intensities with respect to each scan. The resulting voxel intensities are directly treated as RGB channels, where R corresponds to FLAIR, G to T1c and B to T2.

We choose to discard the T1 modality without enhanced contrast instead of any other because this modality is rarely used by radiotherapists to delineate tumor boundaries. Furthermore, the privately acquired dataset presented in Section V does not contain T1 scans.

A novelty of our architecture is that we extend the 3x3 convolutions inside ResNet34 with 1x3x3 convolutions. Since the number of parameters stays the same, pretrained ResNet34 weights can still be loaded without modification. However, the effect is that the architecture is able to treat volumes of any depth now. The encoder simply processes the volumetric data slice-wise.

We add 3x1x1 convolutional depth layers in the upsampling path in order to exploit segmentation correlations in stacks of slices. The depth dimension can be changed to values different from 3 without further adaptation since the depth of the input is not reduced by this convolutional layer thanks to input padding. The architecture can be easily reduced to process slices instead of volumes by disabling the depth layers and choosing an input volume depth of one.

The last layer is a softmax over four channels where the channels correspond to the segmentation labels (edema, tumor core, enhancing tumor and background). Therefore, a single forward pass yields segmentations for all segmentation classes.

B. Loss Function

We use the Multiple Dice Loss as in [6] as a training objective:

$$DSC = \frac{2 \sum_n r_{ln} p_{ln}}{\sum_n r_{ln} + \sum_n p_{ln}} \quad (1)$$

$$\mathcal{L}_{DSC} = 1 - \frac{1}{K} \sum_{l=1}^K DSC \quad (2)$$

where r_{ln} is the reference segmentation and p_{ln} the predicted segmentation for voxel n and class l . DSC is the dice score coefficient that measures the similarity over two sets and can take on values between 0 (minimum) and 1 (maximum). Since there are three segmentation classes without background, we have $K = 3$. The Multiple Dice Loss guarantees equal importance to each class irrespective of their proportion inside the scan. Using multiplications instead of set intersections and additions instead of set unions makes the dice loss function differentiable.

C. Choice of Hyperparameters

The batch size as well as the input patch size are determined by our hardware setup where we occupy the maximum amount of memory possible in order to speed up the training process and to exploit the trade-off between fast and well-directed weight updates.

For the case of 2D inputs, we use randomly sampled patches of 1x128x128 voxels, which leads to a batch size of 64. For the 3D case, we use a patch size of 24x128x128 voxels and a batch size of 24. The patch width and height are chosen to be roughly half of the input dimension of the data provided by the BraTS benchmark. However, it has to be noted that the brain of the patient only occupies a part of the space so that 128x128 patches cover a great part of it.

We use the Adam optimizer with a learning rate of 10^{-3} which yielded the best results in a preliminary evaluation. Training is carried out over 50 epochs where each epoch contains 100 input batch samples drawn uniformly at random from the non-zero area of the MRI input volumes.

Since we make use of data augmentation to improve generalization error, we do not apply any weight decay.

D. Preprocessing and Data Augmentation

We normalize each voxel inside an input channel for each patient. Moreover, we crop the MRI input values to their non-zero regions in order to sample more efficiently and to reduce the memory footprint.

Finally, we apply a set of spatial transforms (data augmentation) to the input patches in order to improve the generalization error. These include elastic deformations, reflections and noise as well as blur. These transformations help the network to deal with unseen low-resolution scans inside the test dataset that occur frequently. The dataloader that we use for data augmentation and preprocessing is publicly available⁵.

E. Prediction

We use the same patch sizes as the ones for training when predicting entire patient volumes. In order to improve prediction performance, we use a sliding window approach where predictions are carried out on overlapping input patches.

⁵<https://github.com/MIC-DKFZ/batchgenerators>

The step sizes of the sliding window are 32 along the width and the height dimension and 24 along the depth dimension of the input. Overlapping predictions are averaged out yielding a slight gain in prediction performance compared to non-overlapping predictions.

IV. DATASETS

A. BraTS'17 and '18 training data

In order to train our models, we use the training data provided by the BraTS'17 and '18 benchmarks [2]. The data has been kept the same in both years and consists of 210 high-grade and 75 low-grade glioma patients. For each patient there exist four types of MRI contrast modalities: T1, T1c (contrast-enhanced), T2 and FLAIR. Each of these contrasts has a resolution of 240x240x155 voxels where the third dimension corresponds to the number of axial slices inside the volumes. The reference tumor segmentations have the same shape as the input volumes and contain annotations for edema, tumor core and the active tumor region (enhancing tumor).

B. BraTS'18 validation data

We use the BraTS'18 validation data to evaluate our models with respect to the BraTS benchmark. The data consists of 66 patients with the same MRI modalities as for the training data. However, it is unknown which patients are high-grade and which are low-grade glioma cases. Moreover, reference annotations are not provided by the organizers. Instead, an online evaluation platform is used that automatically evaluates predicted segmentations. In spite of its name, we do not use this data for a validation of our hyperparameter configurations, but treat the data like a test set. Hyperparameter tuning is carried out on 20% of the training data where the split is done between patients.

C. Clinical dataset of the Syrian-Lebanese hospital

We acquired a private dataset of 25 glioma patients from the Syrian-Lebanese hospital in Brasilia (Brazil). The types of available MRI contrasts as well as their resolutions vary among patients. We selected 5 of these patients by hand for which T1c, T2 and FLAIR MRI modalities were provided. For none of the patients, the T1 modality used in the BraTS benchmark was available. Two of the five patients have two different T1c modalities, a volumetric one with a high depth resolution and a shallow one with a high axial resolution.

A great part of this work was to reverse-engineer the BraTS data preprocessing pipeline and to apply it to the 5 aforementioned patients. This pipeline includes the following steps:

- Conversion of MRI data as well as annotations from DICOM to NIFTI format using 3D Slicer⁶. The NIFTI format joins the files of separate DICOM slices into a single MRI data volume that allows for direct data processing.
- Conversion of each volume to an axial orientation using `fslswapdim` of the FMRIB Software Library (FSL) [24].

- Application of medical brain mask annotations to each scan in order to remove the skull of the patient. This step was done in Python.
- Rigid Co-Registration of each brain volume to a reference scan that had the highest resolution (volumetric T1c in all cases) using nearest-neighbor interpolation. This was done using the FSL FLIRT linear co-registration tool [25].
- Resampling of all volumes and segmentations to an isotropic resolution (1mm x 1mm x 1mm) using nearest-neighbour interpolation. This step was done in Python.

Fig. 3 shows each step of the pipeline. It can be seen that the T1c volumetric scan has axial slices with a lower height than the other MRI modalities. This is due to the fact that less slices were captured in the direction perpendicular to the sagittal plane leading to a lower resolution. However, the overall resolution of the T1c volumetric scan remains the highest. This is because the scan has a high resolution along the direction perpendicular to the axial plane and therefore has a high volume depth. For this reason, all scans were co-registered to the volumetric T1c modality in step (d). The resampling step (e) aligns each voxel with a 1mm³ real-world resolution, which results in naturally looking brain shapes.

For three of our five patients, only one T1c modality was available. This did not change the preprocessing in any way. The only difference is that there are only three modalities (volumetric T1c, T2 and FLAIR) instead of four (volumetric T1c, T1c, T2 and FLAIR).

For the evaluation in Section V, the baseline method requires four input channels. For all patients, we treated the volumetric T1c scan as a T1 channel input to account for the missing T1 data. In the three cases where only one T1c modality was available we used this modality for both the T1 and the T1c input channel.

V. EVALUATION

We evaluate *AlbuNet* (from now on denoted as *AlbuNet2D*) as well as our proposed extension (*AlbuNet3D*) with and without pretraining. Moreover, we compare these models to a baseline (*UCL-TIG*) on the BraTS'18 benchmark (for all segmentation labels) as well as on a privately acquired clinical dataset. For the private clinical dataset we only have access to the tumor core labels.

We choose the dice coefficient as our evaluation metric:

$$DSC = 2 \frac{|A \cap B|}{|A| + |B|} \quad (3)$$

A and B refer to two sets where one contains the voxels of the reference segmentation and the other one the predicted voxels. We calculate the dice coefficient with respect to every segmentation label.

A. Baseline Method - UCL-TIG

We choose the approach developed in [16] as a baseline for our evaluation. This method is an extended version of the second rank solution proposed in BraTS'17 and is currently

⁶<https://www.slicer.org/>

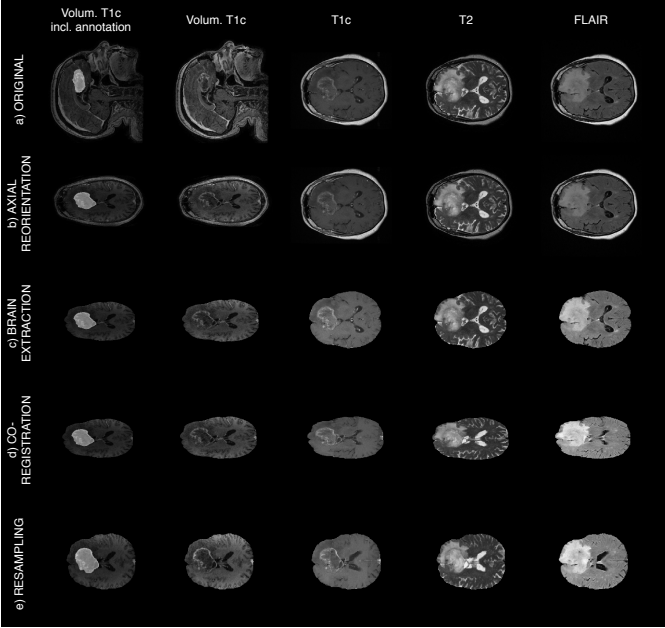


Fig. 3. Illustration of the data preprocessing pipeline that was used to convert the clinical MRI scans into standardized input volumes. The volumetric T1c scan is converted into an axial orientation along with the tumor core annotation (b). The skull of each MRI contrast is removed (c) and the volumes are co-registered to the volumetric T1c scan that has the highest overall resolution (d). Finally, all volumes are resampled to an isotropic resolution (e).

holds for the means and medians of the other segmentation labels.

TABLE I
MEAN (MEDIAN) DICE SCORES FOR THE BRAITS'18 VALIDATION DATA

Method	Whole Tumor	Tumor Core	Enh. Tumor
UCL-TIG	0.9030 (0.9146)	0.8542 (0.9004)	0.7923 (0.8642)
AlbuNet3D (pretr.)	0.8919 (0.9135)	0.8152 (0.9052)	0.7816 (0.8544)
AlbuNet3D (no pretr.)	0.8913 (0.9135)	0.8072 (0.8992)	0.7631 (0.8509)
AlbuNet2D (pretr.)	0.8888 (0.9106)	0.7969 (0.8934)	0.7449 (0.8374)
AlbuNet2D (no pretr.)	0.8774 (0.8992)	0.7776 (0.8762)	0.7437 (0.8331)

Table II shows the evaluation results of five selected patients from our privately acquired clinical dataset whose scans were the most compatible with the BraTS challenge. The overall average performance (AVG) drops for all methods compared to the BraTS'18 evaluation in Table I, which shows that it is not straightforward to apply existing methods to new clinical data. Moreover, it is interesting to note that the pretrained versions of *AlbuNet2D* and *AlbuNet3D* now outperform *UCL-TIG* (higher average dice scores). This is most-likely due to the fact that our methods were only trained on the contrasts available for the clinical dataset. For *UCL-TIG*, we had to replace the T1 contrast with an additional T1c contrast.

The effect of pretraining on the clinical dataset is even larger than the one on the public dataset. This means that pretraining not only induces more robustness to the training process but also to the predictions for previously unseen data that may

be very different from the training data. This can be seen in particular with patient 3 (P3). For this case, the dice score is about 10% higher for the *AlbuNet3D* and about 17% higher for the *AlbuNet2D* version with pretraining compared to the one without.

TABLE II
TUMOR CORE DICE SCORES FOR FIVE PATIENTS (P1-P5) OF THE SYRIAN-LEBANESE HOSPITAL.

Method	P1	P2	P3	P4	P5	AVG
UCL-TIG	0.7795	0.8184	0.4197	0.8238	0.7867	0.7256
AlbuNet3D (pretr.)	0.8580	0.8164	0.4679	0.8158	0.7881	0.7493
AlbuNet3D (no pretr.)	0.8311	0.7902	0.3632	0.8187	0.7812	0.7169
AlbuNet2D (pretr.)	0.8516	0.8156	0.4105	0.8259	0.8000	0.7407
AlbuNet2D (no pretr.)	0.8588	0.8102	0.2411	0.8042	0.7824	0.6993

VI. CONCLUSION

A. Theoretical Implications

Brain tumor segmentation is a very challenging task that is still carried out by humans. However, there is a high demand for automatic segmentation methods that have benefited a lot from recent research in deep learning.

We have shown that encoders pretrained on ImageNet improve the segmentation results of U-Net based architectures for the task of brain tumor segmentation and that they lead to more robust predictions, especially when the test data is different from the training data. In this context, we could simply treat three of the four MRI modalities as RGB input channels of the pretrained encoder architecture and achieve meaningful results. Moreover, we successfully extended *AlbuNet2D* to process volumetric input patches and showed that *AlbuNet3D* yields further performance improvements.

In order to outperform the state-of-the-art on the BraTS benchmark, future research should focus on the question of how to extend our method to all four input channels (T1, T1c, T2 and FLAIR). In this regard it would be possible to train an ensemble where each network uses a three-channel subset of the four provided channels. Another option would be to pretrain a model on four input channels, preferably on a large MRI dataset.

B. Practical Implications

The automatic segmentation results of state-of-the-art methods on the BraTS data are of the same quality as manual segmentations produced by human experts, i.e. *UCL-TIG* achieves mean dice scores of 0.854 for tumor core segmentation compared to 0.86 achieved on average by a human rater [2]. In this regard, the human rater performance is slightly overestimated because it influences the ground truth segmentation labels that were determined by a majority-voting scheme of only four human raters.

However, the MRI data available in a practical clinical context is much more heterogeneous than in the BraTS benchmark. Only a subset of the MRI modalities may be available

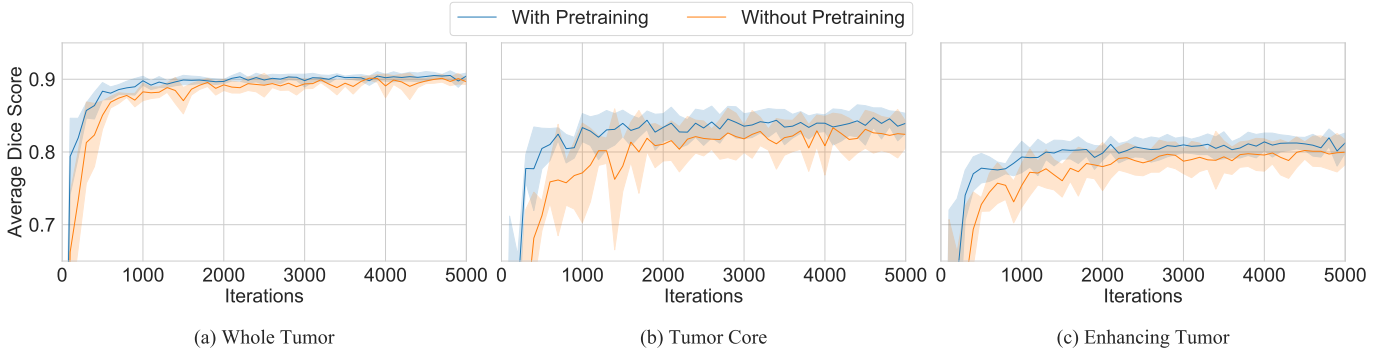


Fig. 4. Validation Dice Scores during training of the AlbuNet3D architecture. We carried out five training runs for the version with and without pretraining, respectively. Thick lines denote the mean dice score over five runs and the shaded error corresponds to the standard deviation from the mean.

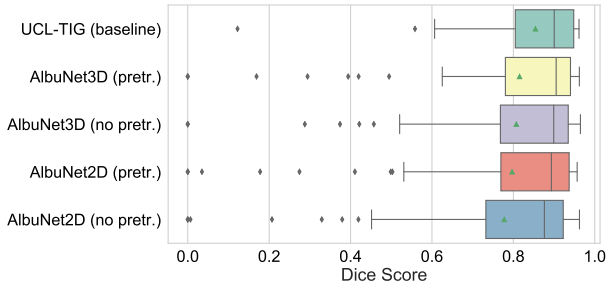


Fig. 5. Boxplot of the tumor core dice scores obtained from the evaluation on the BraTS'18 validation data. The green triangles denote the mean dice score of each method.

for a patient and scans vary strongly in resolution, contrast and orientation. Therefore, it is crucial to develop methods that are able to deal with cases where only a subset of the presented MRI modalities is available. We have shown that pretraining on ImageNet makes the model predictions more robust to these challenges.

Regarding the prediction time of only 15 seconds per patient on a recent GPU, the *AlbuNet3D* method presented in this work could be used in a practical use-case scenario. The CPU prediction time would be higher, but predictions could take place in advance on a remote server. This is feasible because patient data of a hospital is commonly stored on a central server and downloaded upon request. A medical expert could then use the precomputed segmentation labels as guidance for the manual segmentation process.

VII. ACKNOWLEDGEMENT

We would like to thank the Syrian-Lebanese hospital in Brasilia for supplying us with MRI data for 25 glioma patients. We also appreciate the guidance that we received from their experts in the oncology department.

REFERENCES

- [1] D. N. Louis, A. Perry, G. Reifenberger, A. von Deimling, D. Figarella-Branger, W. K. Cavenee, H. Ohgaki, O. D. Wiestler, P. Kleihues, and D. W. Ellison, "The 2016 World Health Organization Classification of Tumors of the Central Nervous System: a summary," *Acta Neuropathologica*, vol. 131, no. 6, pp. 803–820, 2016.
- [2] B. H. Menze *et al.*, "The Multimodal Brain Tumor Image Segmentation Benchmark (BRATS)," *IEEE Transactions on Medical Imaging*, vol. 34, no. 10, pp. 1993–2024, 2015.
- [3] S. Bakas *et al.*, "Advancing The Cancer Genome Atlas glioma MRI collections with expert segmentation labels and radiomic features," *Scientific Data*, vol. 4, no. July, pp. 1–13, 2017. [Online]. Available: <http://dx.doi.org/10.1038/sdata.2017.117>
- [4] O. Ronneberger, P. Fischer, and T. Brox, "U-Net: Convolutional Networks for Biomedical Image Segmentation," pp. 1–8, 2015. [Online]. Available: <http://arxiv.org/abs/1505.04597>
- [5] F. Milletari, N. Navab, and S.-A. Ahmadi, "V-Net: Fully Convolutional Neural Networks for Volumetric Medical Image Segmentation," pp. 1–11, 2016. [Online]. Available: <http://arxiv.org/abs/1606.04797>
- [6] F. Isensee, P. Kickingereder, W. Wick, M. Bendszus, and K. H. Maier-Hein, "Brain tumor segmentation and radiomics survival prediction: Contribution to the BRATS 2017 challenge," *Lecture Notes in Computer Science*, vol. 10670 LNCS, pp. 287–297, 2018.
- [7] O. Russakovsky, J. Deng, H. Su, J. Krause, S. Satheesh, S. Ma, Z. Huang, A. Karpathy, A. Khosla, M. Bernstein, A. C. Berg, and L. Fei-Fei, "ImageNet Large Scale Visual Recognition Challenge," *International Journal of Computer Vision*, vol. 115, no. 3, pp. 211–252, 2015. [Online]. Available: <http://dx.doi.org/10.1007/s11263-015-0816-y>
- [8] V. Iglovikov and A. Shvets, "TernausNet: U-Net with VGG11 Encoder Pre-Trained on ImageNet for Image Segmentation," 2018. [Online]. Available: <http://arxiv.org/abs/1801.05746>
- [9] B. Menze, A. Jakab, and S. Bauer, "BraTS 2013," *Proceedings of MICCAI-BRATS*, 2013.
- [10] A. Pinto, S. Pereira, H. Correia, J. Oliveira, D. M. Rasteiro, and C. A. Silva, "Brain Tumour Segmentation based on Extremely Randomized Forest with high-level features," *Proceedings of the Annual International Conference of the IEEE Engineering in Medicine and*

- Biology Society, EMBS*, vol. 2015–November, pp. 3037–3040, 2015.
- [11] N. J. Tustison, K. L. Shrinidhi, M. Wintermark, C. R. Durst, B. M. Kandel, J. C. Gee, M. C. Grossman, and B. B. Avants, “Optimal Symmetric Multimodal Templates and Concatenated Random Forests for Supervised Brain Tumor Segmentation (Simplified) with ANTsR,” *Neuroinformatics*, vol. 13, no. 2, pp. 209–225, 2015.
- [12] J. Long, E. Shelhamer, and T. Darrell, “Fully convolutional networks for semantic segmentation,” in *CVPR*, 2015, pp. 3431–3440.
- [13] I. Arganda-Carreras *et al.*, “Crowdsourcing the creation of image segmentation algorithms for connectomics,” *Frontiers in Neuroanatomy*, vol. 9, no. November, pp. 1–13, 2015. [Online]. Available: <http://journal.frontiersin.org/Article/10.3389/fnana.2015.00142/abstract>
- [14] V. Ulman *et al.*, “An objective comparison of cell-tracking algorithms,” *Nature Methods*, vol. 14, no. 12, pp. 1141–1152, 2017. [Online]. Available: <http://dx.doi.org/10.1038/nmeth.4473>
- [15] B. Kayalibay, G. Jensen, and P. van der Smagt, “CNN-based Segmentation of Medical Imaging Data,” 2017. [Online]. Available: <http://arxiv.org/abs/1701.03056>
- [16] G. Wang, W. Li, S. Ourselin, and T. Vercauteren, “Automatic Brain Tumor Segmentation using Cascaded Anisotropic Convolutional Neural Networks,” pp. 1–12, 2017. [Online]. Available: <http://arxiv.org/abs/1709.00382>
- [17] A. S. Razavian, H. Azizpour, J. Sullivan, and S. Carlsson, “CNN features off-the-shelf: An astounding baseline for recognition,” *IEEE Computer Society Conference on Computer Vision and Pattern Recognition Workshops*, pp. 512–519, 2014.
- [18] A. A. Shvets, A. Rakhlin, A. A. Kalinin, and V. I. Iglovikov, “Automatic Instrument Segmentation in Robot-Assisted Surgery Using Deep Learning,” *CoRR*, 2018.
- [19] M. Talo, U. Baloglu, O. Yildirim, and U. R. Acharya, “Application of deep transfer learning for automated brain abnormality classification using mr images,” *Cognitive Systems Research*, 12 2018.
- [20] *Transfer Learning for Domain Adaptation in MRI: Application in Brain Lesion Segmentation*, vol. 20, no. Pt3, 2017.
- [21] J. Stawiaski, “A pretrained densenet encoder for brain tumor segmentation,” *ArXiv*, vol. abs/1811.07542, 2018.
- [22] K. He, X. Zhang, S. Ren, and J. Sun, “Deep Residual Learning for Image Recognition,” *ICCV*, 2015. [Online]. Available: <http://arxiv.org/abs/1512.03385>
- [23] A. Shvets, V. Iglovikov, A. Rakhlin, and A. A. Kalinin, “Angiodysplasia detection and localization using deep convolutional neural networks,” *CoRR*, vol. abs/1804.08024, 2018. [Online]. Available: <http://arxiv.org/abs/1804.08024>
- [24] M. Jenkinson, C. F. Beckmann, T. E. Behrens, M. W. Woolrich, and S. M. Smith, “Fsl,” *NeuroImage*, vol. 62, no. 2, pp. 782–790, 2012.
- [25] M. Jenkinson and S. Smith, “Global optimisation method for robust affine registration of brain images,” *Medical image analysis*, vol. 5, pp. 143–56, 07 2001.
- [26] K. He, “Delving Deep into Rectifiers : Surpassing Human-Level Performance on ImageNet Classification,” 2014.
- [27] F. Yu and V. Koltun, “Multi-Scale Context Aggregation by Dilated Convolutions,” 2015. [Online]. Available: <http://arxiv.org/abs/1511.07122>



Jonas Wacker was born in Frankfurt/Main, Germany in 1991. He received his B.S. degree in Information Systems from Technische Universität Darmstadt in 2016. He completed his M.S. degree in Data Science at EURECOM in France in 2018 where he is currently pursuing a Ph.D. degree in Machine Learning. His research evolves around Bayesian Deep Learning methods applied to a novel optical hardware with applications in environmental/life sciences.



Marcelo Ladeira was born in Belo Horizonte/Minas Gerais, Brazil in 1953. He received his Bachelor Science in Mechanical Engineering from University of Brasília, in 1976, and his M.Sc in Systems Analysis from National Institute of Space Research, Brazil, in 1979. After that he worked for eleven years as an Energy Planning Engineer in the Brazilian electrical sector. He is Ph.D. in Computer Science from Federal University of Rio Grande do Sul, Brazil, in 1999. He proposed and was the first software architecture of UnBBayes, an open source Java framework for probabilistic reasoning with probabilistic network. UnBBayes is used by several researchers around the world. Now, his research interests evolve the use of Evolutionary Computation, Data Mining, and Deep Learning to solve real problems.



Jose Eduardo Vaz Nascimento was born in Moca/São Paulo, Brazil, in 1987. He graduated in Medical Physics at the São Paulo University in 2010 and completed his radiotherapy clinical training in 2012 at the Syrian-Lebanese Hospital. He is a certified Radiation Protection Supervisor and Medical Physics Specialist and now he is pursuing Master Degree in Data Science at University of Brasília.